

The Role of Substrate Roughness in Superfluid Film Flow Velocity

Jun Usami · Nobuyuki Kato, Tomohiro Matsui, Hiroshi Fukuyama

Received: date / Accepted: date

Abstract It is known that the apparent film flow rate j_0 of superfluid ^4He increases significantly when the container wall is contaminated by a thin layer of solid air. However, its microscopic mechanism has not yet been clarified enough. We have measured j_0 under largely different conditions for the container wall in terms of surface area ($0.77\text{--}6.15\text{ m}^2$) and surface morphology using sintered silver fine powders (particle size: $0.10\text{ }\mu\text{m}$) and porous glass (pore size: $0.5, 1\text{ }\mu\text{m}$). We could increase j_0 by more than two orders of magnitude compared to non-treated smooth glass walls, where liquid helium flows down from the bottom of container as a continuous stream rather than discrete drips. By modeling the surface morphology, we estimated the effective perimeter of container L_{eff} and calculated the flow rate j ($= j_0 L_0 / L_{\text{eff}}$), where L_0 is the apparent perimeter without considering the microscopic surface structures. The resultant j values for the various containers are constant each other within a factor of four, suggesting that the enhancement of L_{eff} plays a major role to change j_0 to such a huge extent and that the superfluid critical velocity, v_c , does not change appreciably. The measured temperature dependence of j revealed that v_c values in our experiments are determined by the vortex depinning model of Schwarz (Phys. Rev. B **31**, 5782 (1986)) with several nm size pinning sites.

Keywords superfluid · film flow · vortex pinning · critical velocity · porous glass

1 Introduction

Film flow is one of the extraordinary phenomena of superfluidity, and is known as a popular demonstration experiment. Below the Lambda transition temperature ($T_\lambda = 2.1768\text{ K}$), liquid ^4He flows out from a container with an open top through

Department of Physics, The University of Tokyo
7-3-1, Hongo, Bunkyo-ku, Tokyo 133-0033, Japan
J. Usami
E-mail: jusami@kelvin.phys.s.u-tokyo.ac.jp

H. Fukuyama
E-mail: hiroshi@phys.s.u-tokyo.ac.jp

a helium thin film adsorbed on the wall [1]. The film thickness is typically of the order of 10 nm [2]. It is known that the apparent flow rate j_0 , the superfluid mass flow per unit time divided by the macroscopic perimeter of the container L_0 , increases dramatically by contaminating the container wall by a thin layer of solid air [3]. Similar but much smaller increases were observed on unpolished metal surfaces such as stainless steel, while flow rates on highly polished ones are nearly the same as that on clean glass [4]. This indicates that j_0 is insensitive to the wall material but dependent on the microscopic structure of the surface.

Smith and Boorse [5] examined the roughness dependence of j_0 for various metal surfaces. Their results are consistent with the model in which the j_0 enhancement is explained only by the geometrical effect, i.e., the effectively extended perimeter due to the roughness (*effective perimeter model*) [3, 6]. However, one can also imagine that j_0 in the air contaminated container may also be enhanced by the dramatic increase of the superfluid critical velocity v_c which could happen for some reason. To test this possibility, it is crucial to estimate the former effect quantitatively. However, it is generally difficult to control and evaluate the surface structure of the thin layer of solid air.

In this paper, we present results of film flow rate measurements of superfluid ^4He using two different types of glass containers, i.e., glass containers covered by layers of sintered silver powders (Type-1) and those with porous surfaces (Type-2), and compared them with published results of bare glass containers [6, 7]. For the surface decorated containers, we observed dramatic increases of j_0 at $T = 2.04$ K by more than two orders of magnitude compared to that for the bare glass containers. Then, we evaluated effectively enhanced perimeters L_{eff} for them by modeling the surface morphology based on scanning electron microscope (SEM) images and surface area measurements. Flow rates j corrected by L_{eff} , i.e., $j = j_0 L_0 / L_{\text{eff}}$, for various containers are consistent with each other within a factor of four. This means that v_c is more or less unchanged regardless of such largely different surface roughness and that the geometrical effect plays a major role on the huge enhancement of j_0 in our experiments and most likely in air contaminated containers as well. The measured temperature dependence of j suggests that v_c is determined by the vortex depinning mechanism [8] with pinning sites smaller than 10 nm.

2 Experimental methods

The Type-1 containers are made of Pyrex glass with dimensions; 28/32 mm in inner/outer diameter and 15 mm in inner height. The rim of an open top of the container (bucket-type) was made as smooth as possible. The whole surface of the container except 10 mm wide vertical slits to observe inner liquid level was covered by a layer of sintered Ag powder of 0.10 μm particle diameter (C-8 Ag powder manufactured by Tokuriki Honten, Co., Ltd.). To fix the Ag powder on the glass surface, they were mixed in a paste containing Ag flakes of ~ 5 μm size and painted on the surfaces by a brush. The weight ratio of Ag powder to paste was 1 (Ag-2) or 5 (others). Then the container was heated in air to sinter the Ag powder at different temperatures of 120, 150 or 180 $^\circ\text{C}$ for 15 or 60 min. We prepared four containers of this type (Ag-1 \sim Ag-4) with different sintering conditions as shown in Table 1.

Table 1 Specifications of various containers. p and q are parameters used in eq.(3) which models the morphology of porous glass. They correspond to the apparent pore and channel diameters, respectively, in the SEM image (see the main text for more details). In the last line, measured apparent flow rates j_0 at $T = 2.05$ K are also shown where the data of the bare glass container is from Ref.[6, 7].

	bare	Type-1				Type-2	
	Glass	Ag-1	Ag-2	Ag-3	Ag-4	PG-1	PG-2
T_{sint} ($^{\circ}\text{C}$)	—	180	180	150	120	—	—
t_{sint} (min)	—	60	60	15	15	—	—
p (μm)	—	—	—	—	—	0.5	1
q (μm)	—	—	—	—	—	0.3	0.5
$j_0 \times 10^5$ (kg/m/s)	0.032	4.7, 13, 19	15	1.6	3.5	3.5	2.2
S (m^2)	0.0044	0.79, 1.70, 2.52	2.81	0.77	1.33	6.2	2.0

SEM images of surfaces of Ag-1 and Ag-4 are shown in Fig. 1. Even at the lowest sintering temperature and for the short sintering time ($T_{\text{sint}} = 120$ $^{\circ}\text{C}$, $t_{\text{sint}} = 15$ min), individual Ag particles and their grains are well connected with each other as seen in Fig. 1(c). At the highest sintering temperature and for the long sintering time (180 $^{\circ}\text{C}$, 60 min), as shown in Fig. 1(a), the inter-particle neck becomes thicker, but the original particle size is still kept not clustering too much. More global connections are seen in Fig. 1(b). In both cases, Ag clusters of a few tens μm size are well connected with each other.

The Type-2 containers are made of phase separated two components of acid-soluble and -insoluble glasses. The dimensions are 16/22 mm in inner/outer diameter and 12 mm in inner height. The outer surfaces of 36 or 50 μm thick were made porous by dissolving the acid-soluble component [9]. We used two kinds of containers, PG-1 and PG-2, of this type with different pore sizes. From SEM observations shown in Figs. 2(a),(b), the pore and channel sizes are estimated as 0.5 and 0.3 μm for PG-1 and 1.0 and 0.5 μm for PG-2, respectively. Structures of the top surface and cross section of the porous layer are similar to each other.

Surface areas (S) of glass pieces prepared in the same way as the Type-1 and -2 containers were determined from the isothermal adsorption pressure measurements of nitrogen molecules at $T = 77$ K. All the specifications of the containers are summarized in Table 1.

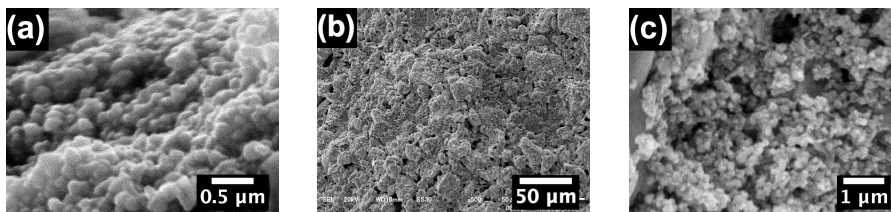


Fig. 1 SEM images of surfaces of (a)(b) Ag-1 and (c) Ag-4 containers of Type-1.

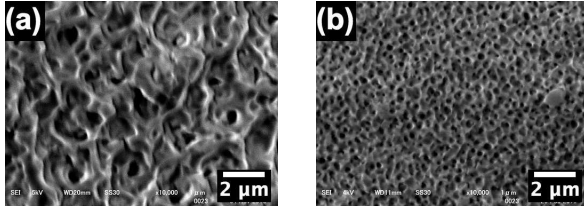


Fig. 2 SEM images of top surfaces of (a) PG-1 and (b) PG-2 containers of Type-2.

The film flow rate j was determined by measuring the time t during which superfluid ^4He of a volume V flows out of each container after lifting it up from the superfluid ^4He bath in a glass dewar. j is given by

$$j = \frac{V\rho}{tL_{\text{eff}}}, \quad (1)$$

where ρ is the density of ^4He . We denote j_0 rather than j when we assume $L_{\text{eff}} = L_0$ in Eq. 1, where L_0 is the nominal perimeter of container determined from its macroscopic shape. For the bare glass container, we can expect $j \approx j_0$.

Since it is not easy to determine the temperature of thin ^4He film itself, various precautions were taken. For example, we kept the container bottom close to the bath level (10 mm above) during the flow measurements, and carefully radiation shielded the container region. Then we assumed that the temperature determined from the ^4He vapor pressure and a calibrated Allen Bradley resistance thermometer (nominal 200 Ω) immersed in the bath is reasonably close to the film temperature. Most of the data were taken at a fixed temperature of $T=2.04(2)$ K. The T -dependence of j was also measured for PG-1 near T_λ ($1.39 \leq T \leq 2.12$ K).

3 Results and discussion

As indicated in Table 1, we observed anomalously large flow rates for Type-1 and -2 containers at $T = 2.04(2)$ K. They are larger than that for bare glass [6, 7] by more than two orders of magnitude, and liquid helium flows continuously like a waterfall from the bottom of the container.

We estimated the effective perimeter L_{eff} by modeling structures of the sintered Ag powder and the porous layers based on the SEM images (Figs. 1 and 2). For Type-1, the model is packed spheres of $2r = 100$ nm in diameter (see Fig. 3(a)). In this model, the total surface area S is given by $4\pi r^2[S_0/(2r)^2][H/2r]$ and L_{eff} is given by

$$L_{\text{eff}} = 2\pi r \frac{H}{2r} \frac{L_0}{2r} = \frac{S}{S_0} L_0 \quad (\text{Model-1}), \quad (2)$$

where H is the thickness of this structure and S_0 is the surface area of a base glass container without the Ag powder. For Type-2, the model is a lattice composed of ring tori (see Fig. 3(b)). A unit cell of the lattice consists of 6 tori forming a cube shape. This is a complementary space left after removing a central sphere from a cube (Fig. 3(c)). This jungle-gym structure is likely expected from the fact that the spherically segregated acid-soluble glass component is removed by the dissolving process. In this model, the surface area of a torus is $\pi^2[(p-q)/2][(p+q)/2]$ and

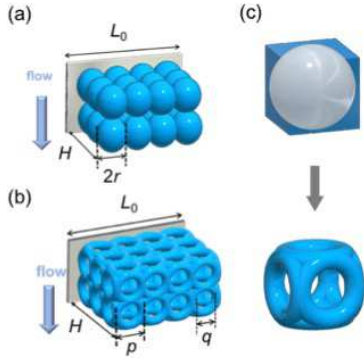


Fig. 3 Schematic drawings of surface structures of (a) Ag powder (Model-1), (b) porous glass (Model-2) and (c) a unit cell in Model-2.

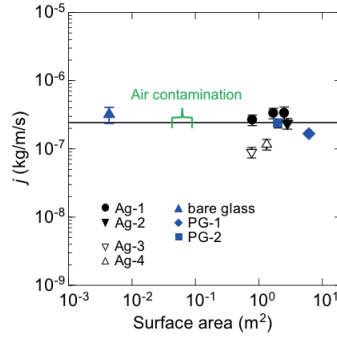


Fig. 4 Flow rate j at $T=2.04$ K versus S . j is obtained through eq.(1) by estimating L_{eff} as described in the main text. The horizontal line shows a theoretical value given by eqs.(4) and (5) with $b = 6$ nm, $c = 0.2$. If the effective perimeter mechanism plays dominant roles in the previous experiments with air contaminated containers [3], they would be located in the region indicated by the green bracket.

thus S/S_0 is given by $(3\pi^2/4)[(p-q)(p+q)H/p^3]$, where p and q are outer and inner diameters of the torus. Then, L_{eff} is given by

$$L_{\text{eff}} = \pi \frac{p-q}{2} \frac{L_0 H}{p^2} = \frac{2}{3\pi} \frac{S}{S_0} \frac{p}{p+q} L_0 \quad (\text{Model-2}). \quad (3)$$

L_{eff} values estimated by these models are tabulated in Table 1.

Using these L_{eff} values, we can deduce j for various containers from Eq.1. They are plotted in Fig. 4 with respect to S . All the j data, except for Ag-3 and 4, fall on the same value within a factor of two. This is a surprisingly good agreement considering such different surface morphology and surface areas over two orders of magnitude. Clearly, the enhancement of v_c has a negligibly small effect on the dramatic increase of j_0 , and v_c changes only a little, within a factor of 3–4 at most, regardless of such largely different surface roughness. In other words, the geometrical effect plays a dominant role on the observed enhancement of ρ_0 in our surface decorated containers, and this must be the most relevant mechanism in the containers contaminated with solid air.

The data for Ag-3 and 4 seem to be systematically smaller than the others approximately by a factor of two (see Fig. 4). This is presumably due to poorer applicability of the Model-2 to the case when insufficient neck grows between adjacent Ag particles due to the lower T_{sint} and the shorter t_{sint} . Such thin neck parts will contribute to overestimate L_{eff} . The He film thickness adsorbed on Ag surfaces should be larger than that on glass surfaces by about 40% because of the stronger Van der Waals attractive force. However, such a small difference is not important in this study where we varied L_{eff} to so large extent.

The film flow rates are nearly independent of the liquid level in our experiment as in the previous works [10, 11]. From this fact it is natural to consider that the

flows are also determined by the superfluid critical velocity v_c . If we assume the constant film thickness η over the whole surface, which is about 30 nm on glass surfaces and is weakly level dependent eventually, $V/t \approx v_c \eta L_{\text{eff}} \rho_s / \rho$. Here ρ_s / ρ is the superfluid fraction which is well tabulated as a function of T in literature [12]. Then Eq. 1 can be rewritten as

$$j(T) = v_c \eta \rho_s(T). \quad (4)$$

and through this relation v_c can be deduced from j .

In the early days, it has been considered that v_c in the film flow is T -independent [10]. However, as far as we know, it has not been reexamined carefully from the view point of subsequent theoretical progress. Among others, the vortex depinning model by Schwarz [8] will be one of the most relevant descriptions for v_c in our experimental setup. In this model, v_c is given by

$$v_c(T) = c \frac{h}{4\pi m \eta} \ln(b/a(T)), \quad (5)$$

where h , m , b , and a are Planck's constant, mass of He atom, typical size of surface pinning sites, and the vortex core radius (~ 0.1 nm). c is a constant of the order of unity. The insensitivity of v_c to the surface decoration we observed can be explained by the logarithmically weak dependence of v_c on b within this model. Since a has weak T -dependence except for close to T_λ [13], the relevancy of the vortex depinning model can be tested if we deduce $v_c(T)$ from j measured at various T near T_λ through Eq. 4 and compare it with Eq. 5.

Eventually, we found a weak but clear T -dependence of v_c for PG-1 container in the whole T region ($1.39 \leq T \leq 2.12$ K) we studied (see Fig. 5). Moreover, the T -dependence of v_c data can be well represented by Eq. 5 with $b = 6$ nm and $c = 0.16$ as indicated by the solid line where we used the T -dependence of a given in Ref. [13]. On the other hand, a fitting to Eq. 5 with $b = 30$ nm (the long dashed dotted line; $c = 0.12$) does not represent the data well. Also, a fitting to another formula $v_c = c\{1 - (T/T_0)\}$, which is proposed by the vortex nucleation mechanism [14, 15], (the dashed line; $c = 0.22$, $T_0 = 2.45$ K) can not represent the data at all. Thus our results strongly suggest that the superfluid film flow is determined by depinning of remnant vortices from pinning sites smaller than

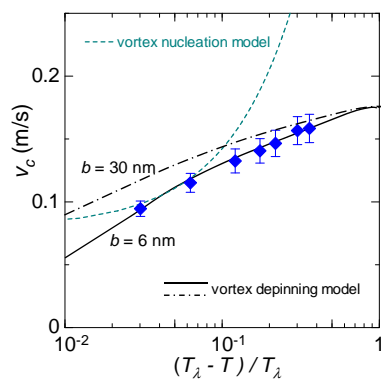


Fig. 5 T -dependence of v_c deduced from the film flow experiment for Type-2 container. Fittings to Eq. 5 with $b = 6$ nm, $c = 0.16$ and $b = 30$ nm, $c = 0.12$ are indicated by the solid line and the dash-dot one, respectively. The dashed line is a fitting to the vortex nucleation model [14, 15]. See text for details.

expectedly for containers made of other materials will be valuable to confirm this conclusion.

Finally, we comment that similarly deduced $v_c(T)$ from j data in the previous film flow experiments scatter too largely to draw a clear conclusion. Some of them seem to show even a stronger T -dependence [16] or almost no dependence [6].

4 Conclusions

We have measured the apparent film flow rate j_0 of superfluid ^4He for glass containers with different surface decorations. With increasing the surface area, i.e., the effective perimeter L_{eff} , we observed a huge enhancement of j_0 by more than two orders of magnitude. By properly evaluating L_{eff} based on the simple models for the surface morphology, we concluded that the enhancement is almost thoroughly caused by the geometrical effect not by the substantial increase of the critical velocity v_c . Larger flow rate of the air contaminated container seems to be explained by the increase of the effective perimeter. From the measurement of temperature dependence of the flow rate, it was strongly suggested that v_c is weakly T dependent in accordance with the vortex depinning mechanism.

Acknowledgements The authors thank Akagawa Glass Co. Ltd. for providing us the porous glass containers. We are also grateful to the late Tadao Imai for processing the Pyrex glass containers. JU was supported by Japan Society for the Promotion of Science through Program for Leading Graduate Schools (MERIT).

References

1. J.G. Daunt, K. Mendelssohn, *Nature* **141**(3577), 911 (1938). DOI 10.1038/141911a0. URL <http://www.nature.com/articles/141911a0>
2. C.W.F. Everitt, K.R. Atkins, A. Denenstein, *Physical Review* **136**(6A), A1494 (1964). DOI 10.1103/PhysRev.136.A1494. URL <https://link.aps.org/doi/10.1103/PhysRev.136.A1494>
3. R. Bowers, K. Mendelssohn, *Proceedings of the Physical Society. Section A* **63**(12), 1318 (1950). DOI 10.1088/0370-1298/63/12/303. URL <http://stacks.iop.org/0370-1298/63/i=12/a=303?key=crossref.be962ad581b38b2a211580a85fddbd9a>
4. B.S. Chandrasekhar, K. Mendelssohn, *Proceedings of the Physical Society. Section A* **65**(3), 226 (1952). DOI 10.1088/0370-1298/65/3/111. URL <http://stacks.iop.org/0370-1298/65/i=3/a=111?key=crossref.5a45b692ae11f9c3c68c27c1b32939d5>
5. B. Smith, H.A. Boorse, *Physical Review* **99**(2), 346 (1955). DOI 10.1103/PhysRev.99.346. URL <https://link.aps.org/doi/10.1103/PhysRev.99.346>
6. K. Mendelssohn, G.K. White, *Proceedings of the Physical Society. Section A* **63**(12), 1328 (1950). DOI 10.1088/0370-1298/63/12/304. URL <http://stacks.iop.org/0370-1298/63/i=12/a=304?key=crossref.f8c9ed9650a563dc731f4c60d2a35e4e>
7. B. Smith, H.A. Boorse, *Physical Review* **98**(2), 328 (1955). DOI 10.1103/PhysRev.98.328. URL <https://link.aps.org/doi/10.1103/PhysRev.98.328>

8. K.W. Schwarz, *Physical Review B* **31**(9), 5782 (1985). DOI 10.1103/PhysRevB.31.5782. URL <https://link.aps.org/doi/10.1103/PhysRevB.31.5782>
9. M. Kukizaki, *Journal of Membrane Science* **360**(1-2), 426 (2010). DOI 10.1016/J.MEMSCI.2010.05.042. URL <https://www.sciencedirect.com/science/article/pii/S0376738810004102>
10. J.G. Daunt, R.S. Smith, *Reviews of Modern Physics* **26**(2), 172 (1954). DOI 10.1103/RevModPhys.26.172. URL <https://link.aps.org/doi/10.1103/RevModPhys.26.172>
11. C.J. Duthler, G.L. Pollack, *Physical Review A* **3**(1), 191 (1971). DOI 10.1103/PhysRevA.3.191. URL <https://link.aps.org/doi/10.1103/PhysRevA.3.191>
12. R.J. Donnelly, C.F. Barenghi, *Journal of Physical and Chemical Reference Data* **27**(6), 1217 (1998). DOI 10.1063/1.556028. URL <http://aip.scitation.org/doi/abs/10.1063/1.556028><http://scitation.aip.org/content/aip/journal/jpcrd/27>
13. C.F. Barenghi, R.J. Donnelly, W.F. Vinen, *Journal of Low Temperature Physics* **52**(3-4), 189 (1983). DOI 10.1007/BF00682247. URL <http://link.springer.com/10.1007/BF00682247>
14. E. Varoquaux, M.W. Meisel, O. Avenel, *Physical Review Letters* **57**(18), 2291 (1986). DOI 10.1103/PhysRevLett.57.2291. URL <https://link.aps.org/doi/10.1103/PhysRevLett.57.2291>
15. B.P. Beecken, W. Zimmermann, *Physical Review B* **35**(4), 1630 (1987). DOI 10.1103/PhysRevB.35.1630. URL <https://link.aps.org/doi/10.1103/PhysRevB.35.1630>
16. J.G. Daunt, K. Mendelssohn, *Proceedings of the Royal Society of London. Series A, Mathematical and Physical Sciences* **170**(942), 439 (1939). URL <http://www.jstor.org/stable/97282>